Porous nickel sulfide nanorods serve as multifunctional electrocatalyst for hydrogen evolution reaction, urea electro-oxidation reaction, and nitrate reduction reaction

Xiaoyu Zhang[a], Jiayi Wang[a], Kai Zong[a], Lin Yang[a], Xin Wang*[a], Zhongwei Chen*[b]

[a]Institute of Carbon Neutrality, Zhejiang Wanli University, Ningbo 315100, China
E-mail: wangx@zwu.edu.cn (X. Wang).
[b]Dalian Institute of Chemical Physics, Chinese Academy of Sciences, Dalian 116023, China
E-mail: zwchen@dicp.ac.cn (Z. Chen)

Electrochemical Measurements

Linear sweep voltammetry (LSV), chronopotentiometry (CP), and electrochemical impedance (EIS) measurements were carried out in a 1.0 M KOH for the OER and HER, 1.0 M KOH+ 0.33 M urea for the UEOR, and 0.5 M Na_2SO_4+ 0.1 M $NaNO_3$ for NO_3RR using CHI 760E workstation. To prepare the catalyst ink, 2.0 mg of the catalyst, 0.2 mL of H_2O, 0.8 mL of C_2H_5OH and 5 μL of Nafion (5 wt%) solution were mixed and ultrasonicated for 30 min. All measurements were performed in a three-electrode configuration at room temperature, using a saturated calomel electrode as the reference electrode and a platinum plate as the counter electrode. All potentials in this work were calibrated to the reversible hydrogen electrode (RHE).

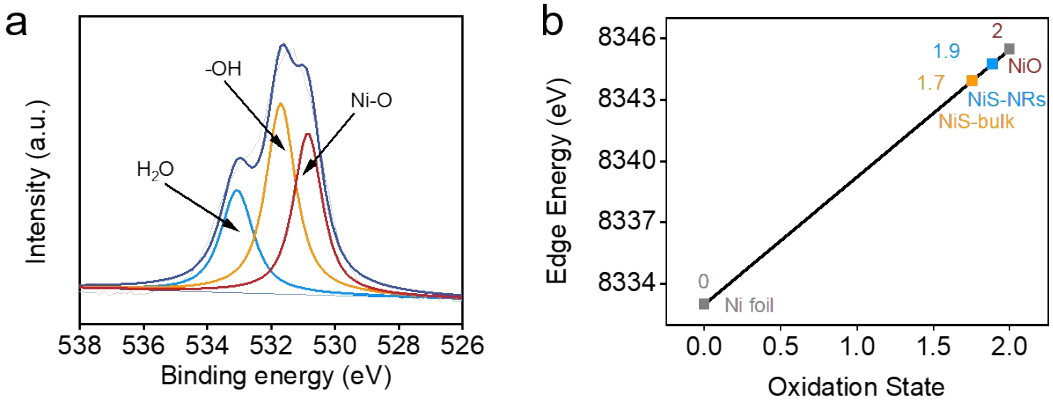

Figure S1 (a) The XPS spectra of O 2p of NiS-NRs. (b) Fitted oxidation states of Ni for NiS-NRs, NiS-bulk, NiO, and Ni foil.

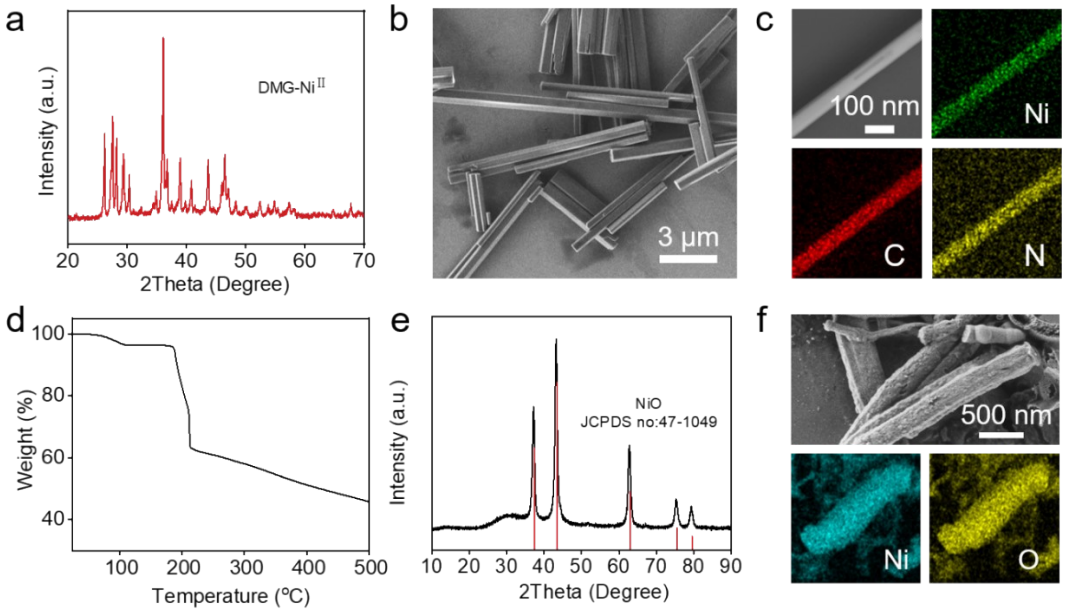

Figure S2 (a) The XRD pattern, (b) SEM image, (c) EDS maps, and (d) TG curve of the DMG-Ni^{II} complex nanorods. (e) The XRD pattern and (f) SEM image of NiO nanorods.

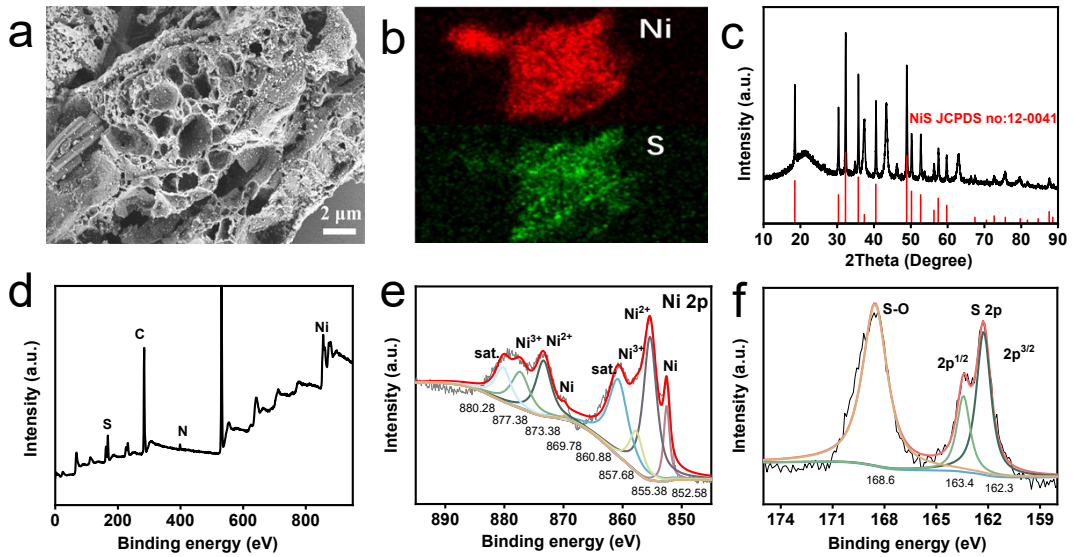

Figure S3 (a) The SEM image, (b) EDX maps, (c) XRD pattern, (d) XPS survey spectrum, (e) Ni 2p XPS spectrum, and (f) S 2p XPS spectrum of NiS-bulk.

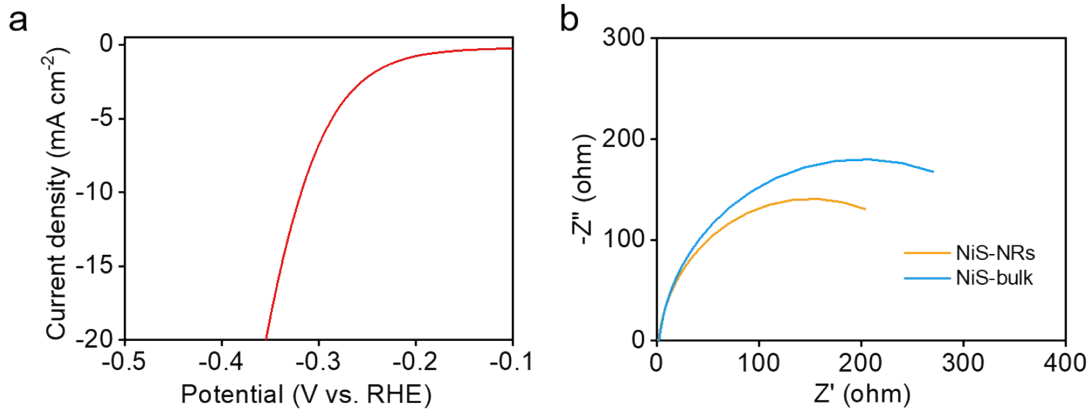

Figure S4 (a) HER performance of NiO. (b) Nyquist plots of the NiS-NRs and NiS-bulk in N_2-saturated 1.0 M KOH electrolyte.

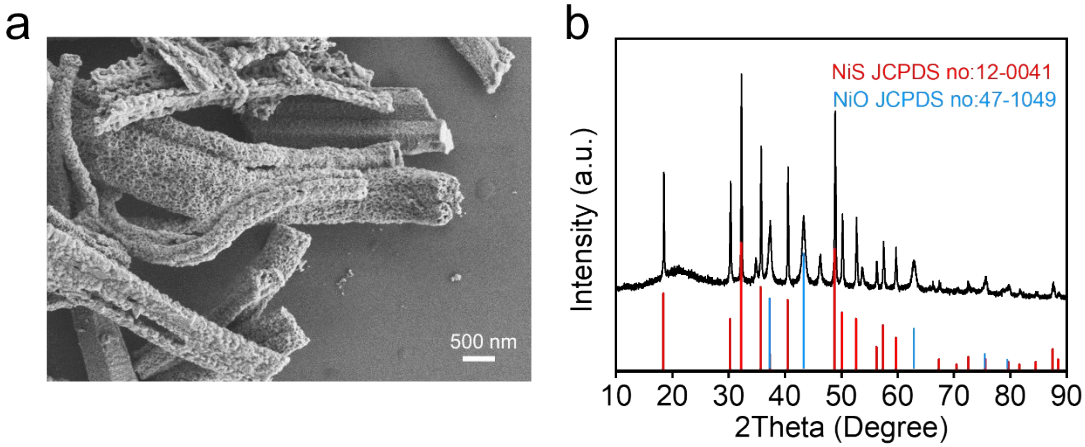

Figure S5 (a) the SEM image and (b) XRD pattern of NiS-NRs after HER stability test.

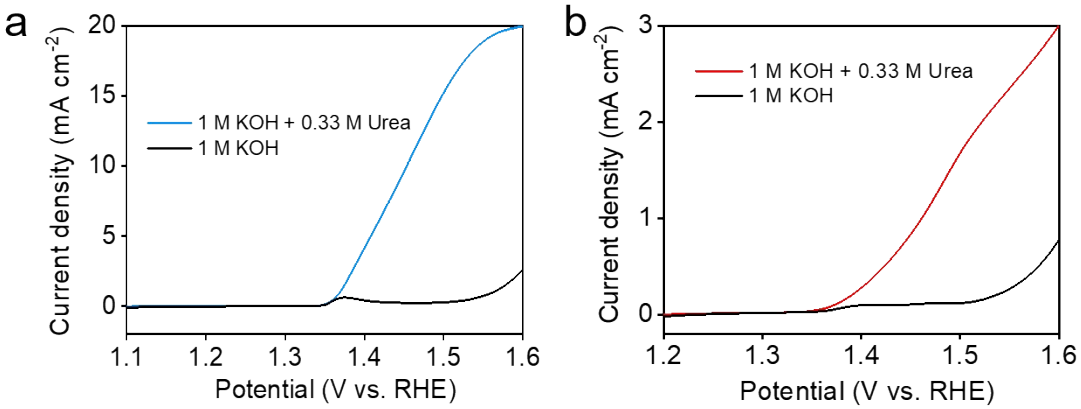

Figure S6 (a) LSV curves of NiS-bulk in N_2-saturated 1.0 M KOH solution with and without 0.33 M urea at 10 mV s^{-1}. (b) LSV curves of NiO in N_2-saturated 1.0 M KOH solution with and without 0.33 M urea at 10 mV s^{-1}.

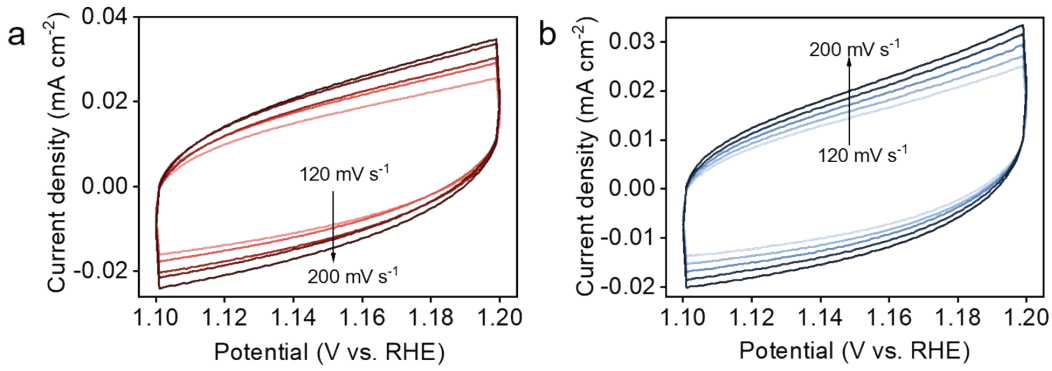

Figure S7 CV curves of (a) NiS-NRs and (b) NiS-Bulk in N_2-saturated 1.0 M KOH solution at different scan rates.

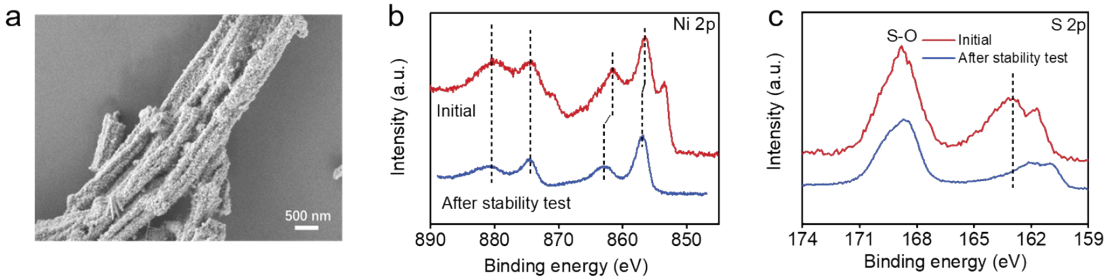

Figure S8 (a) The SEM image of the NiS-NRs catalyst after the stability test. XPS spectra of (b) Ni 2p and (c) S 2p of NiS-NRs catalyst before and after stability test.

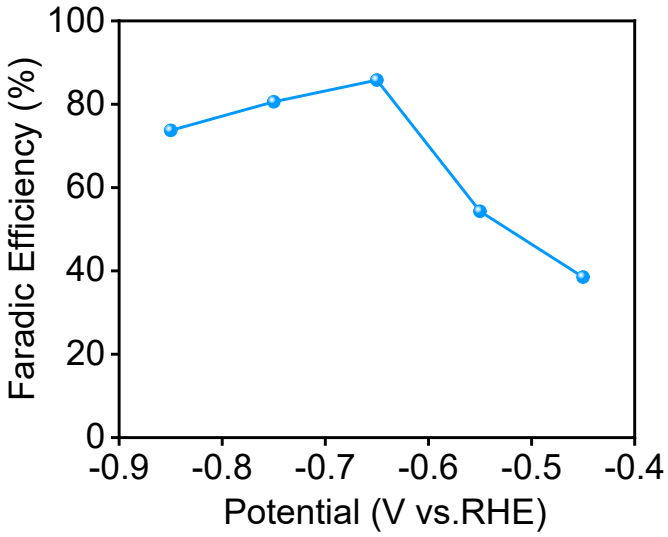

Figure S9 Potential-dependent Faradaic efficiency of NH_3 on NiS-NRs.

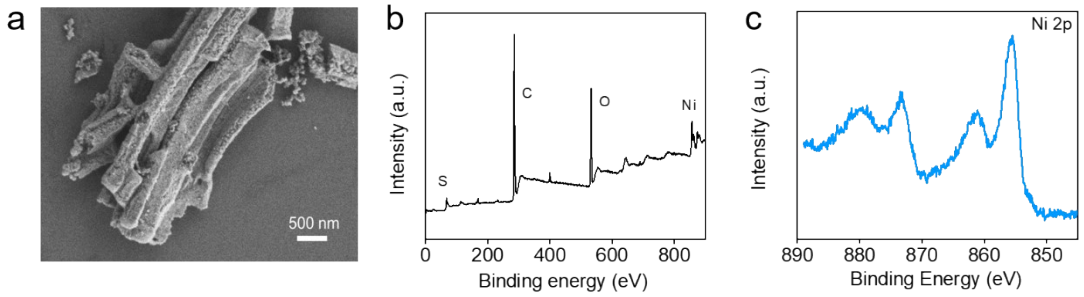

Figure S10 (a) The SEM image of the NiS-NRs catalyst after NO_3RR test. (b) XPS full-scan survey spectrum of NiS-NRs after NO_3RR test. (c) XPS spectra of Ni 2p of NiS-NRs catalyst after NO_3RR test.

Table S1 Comparison of the electrochemical performance of Ni-based electrocatalysts in UEOR.

Electrocatalysts	Electrolyte	UEOR j_{10} (V)	Urea electrolyzer j_{10} (V)	Ref.
NiS nanorods	1.0 M KOH + 0.33 M Urea	1.37	1.41	This work
$NiSe_2/MoSe_2$	1.0 M KOH + 0.33 M Urea	1.34	1.44	1
NiSe	1.0 M KOH + 0.33 M Urea	1.40	1.47	2
NiS nanotube	1.0 M KOH + 0.33 M Urea	1.36	1.445	3
NiS@Ni-CNFs	1.0 M KOH + 0.33 M Urea	1.366	1.44	4
Fe-doped NiS-NiS2	1.0 M KOH + 0.33 M Urea	1.34	1.55	5
O_{vac}-V-$Ni(OH)_2$	1.0 M KOH + 0.33 M Urea	1.38	1.50	6
Ir-NiFe-OH	1.0 M KOH + 0.33 M Urea	1.36	1.42	7
Fe-$NiSe_2$	1.0 M KOH + 0.33 M Urea	1.38	1.45	2
Ni_3S_2-Ni_3P/NF	1.0 M KOH + 0.33 M Urea	1.37	1.43	8

Table S2 Comparison of the electrochemical performance of Ni-based electrocatalysts in NO_3RR

Electrocatalysts	Electrolyte	Onset potential (V)	NH_4 yield (mmol h^{-1} mg_{cat}^{-1})	Ref.
NiS nanorods	0.5 M SO_4^{2-}+0.1 M NO_3^-	-0.42	0.513	This work
Ni_2P	0.5 M SO_4^{2-}+0.05 M NO_3^-	-0.6	0.056	9
CuNi	0.1 M PBS + 0.5 mg mL^{-1} NO_3^-	-0.8	0.3659	10
CuNi solid solution alloys	1 M KOH +0.1 M NO_3^-	0.1	0.264	11
Cu/Ni- N-doped carbon	0.5 M SO_4^{2-} + 0.1 mg mL^{-1} NO_3^-	-0.46	0.324 mmol h^{-1} cm^{-2}	12
BCN@Ni	0.1 M KOH + 0.1 M NO_3^-	0	0.1365 mmol h^{-1} cm^{-2}	13
$Cu_{0.25}Ni_{0.25}$	1 M KOH + 0.075 M NO_3^-	0.18	0.5496 mmol h^{-1} cm^{-2}	14

Reference

1. X. Xu, H. Liao, L. Huang, et al., Surface reconstruction and directed electron transport in $NiSe_2/MoSe_2$ Mott-Schottky heterojunction catalysts promote urea-assisted water splitting, *Appl. Catal., B: Environ.*, 2024, **341**, 123312.
2. L. Yu, X. Pang, Z. Tian, et al., Fe-doped $NiSe_2$ nanorods for enhanced urea electrolysis of hydrogen generation, *Electrochimica Acta*, 2023, **440**, 141724.
3. M. Zhong, W. Li, C. Wang, et al., Synthesis of hierarchical nickel sulfide nanotubes for highly efficient electrocatalytic urea oxidation, *Applied Surface Science*, 2022, **575**, 151708.
4. M. Zhong, J. Yang, M. Xu, et al., Significantly Enhanced Energy-Saving H_2 Production Coupled with Urea Oxidation by Low- and Non-Pt Anchored on NiS-Based Conductive Nanofibers, *Small*, 2024, **20**, e2304782.
5. S. Huang, Q. Zhang, P. Xin, et al., Construction of Fe-doped NiS-NiS_2 Heterostructured Microspheres Via Etching Prussian Blue Analogues for Efficient Water-Urea Splitting, *Small*, 2022, **18**, e2106841.
6. H. Qin, Y. Ye, J. Li, et al., Synergistic Engineering of Doping and Vacancy in $Ni(OH)_2$ to Boost Urea Electrooxidation, *Adv Funct Mater*, 2022, **33**, 2209698.
7. X. Chen, J. Wan, J. Chai, et al., Nickel-iron in the second coordination shell boost single-atomic-site iridium catalysts for high-performance urea electrooxidation, *Nano Research*, 2024, **17**, 3919-3926.
8. J. Liu, Y. Wang, Y. Liao, et al., Heterostructured Ni_3S_2-Ni_3P/NF as a Bifunctional Catalyst for Overall Urea-Water Electrolysis for Hydrogen Generation, *ACS Applied Materials & Interfaces*, 2021, **13**, 26948-26959.
9. Q. Yao, J. Chen, S. Xiao, et al., Selective Electrocatalytic Reduction of Nitrate to Ammonia with Nickel Phosphide, *ACS Appl Mater Interfaces*, 2021, **13**, 30458-30467.
10. J. Zhao, L. Liu, Y. Yang, et al., Insights into Electrocatalytic Nitrate Reduction to Ammonia via Cu-Based Bimetallic Catalysts, *ACS Sustainable Chem Eng*, 2023, **11**, 2468-2475.
11. Y.-Y. Lou, Q.-Z. Zheng, S.-Y. Zhou, et al., Phase-dependent Electrocatalytic Nitrate Reduction to Ammonia on Janus Cu@Ni Tandem Catalyst, *ACS Catal*, 2024, **14**, 5098-5108.
12. Y. Wang, H. Yin, F. Dong, et al., N-Coordinated Cu-Ni Dual-Single-Atom Catalyst for Highly Selective Electrocatalytic Reduction of Nitrate to Ammonia, *Small*, 2023, **19**, e2207695.
13. X. Zhao, Z. Zhu, Y. He, et al., Simultaneous anchoring of Ni nanoparticles and single-atom Ni on BCN matrix promotes efficient conversion of nitrate in water into high-value-added ammonia, *Chem Eng J*, 2022, **433**, 133190.
14. J. Wang, L. Zhang, Y. Wang, et al., Facet and d-band center engineering of CuNi nanocrystals for efficient nitrate electroreduction to ammonia, *Dalton Trans*, 2022, **51**, 15111-15120.